IV International Conference on Particle-based Methods – Fundamentals and Applications
PARTICLES 2015
E. Oñate, M. Bischoff, D.R.J. Owen, P. Wriggers & T. Zohdi (Eds)

INVESTIGATIONS OF VORTEX STRUCTURES IN GRANULAR MATERIALS UNDER EARTH PRESSURE CONDITIONS BY DEM

MICHAŁ NITKA AND JACEK TEJCHMAN

Faculty of Civil and Environmental Engineering
Gdańsk University of Technology, Gdańsk, Poland
micnitka@pg.gda.pl, tejchmk@pg.gda.pl

Key words: DEM, Earth Pressure, Granular Materials, Shear Zone, Vortex.

Abstract. The evolution of shear zones in initially medium dense cohesionless sand for quasi-static earth pressure problems of a retaining wall was analysed with a 3D discrete element method DEM using spheres with contact moments. The passive sand failure for a very rough retaining wall undergoing horizontal translation was discussed. Attention was paid to vortex and anti-vortex structures appearing in granular shear zones. Three different methods were introduced to find granular vortices.

1 INTRODUCTION

The granular vortex structures (swirling motion of several grains around its central point) are frequently observed in experiments on dense granular materials - they are a direct manifestation of grain rearrangement and therefore they can be thought of as a basic mechanism of irreversible deformation [1-3]. They become apparent when the motion associated with uniform (affine) strain is subtracted from the actual granular deformation. They are reminiscent of turbulence in fluid dynamics (Radjai and Roux) [4], however the amount of the grain rotation is several ranges of magnitude smaller (~0.01^o - 0.1^o) than the fluid vortex rotation and granular flow is too slow to induce inertial force characteristic for turbulences in fluid. They were studied by means of the discrete element method (DEM) by many researchers. The vortices are regarded as playing a strong role in heat convection in dry granular flows [5] and in reducing the amount of frictional dissipation in fault gouges [6]. According to Peters and Walizer [7] vortices represent an independent flow field following its own governing equations and satisfying its own (null) boundary conditions. The dominant mechanism responsible for vortex formation was the buckling of force chains [8], [9]. The collapse of main force chains leads to the formation of larger voids and their build-up to the formation of smaller voids [9].

In general, it is difficult to say at this stage of research whether vortex structures have any significant impact on the granular matter and how they could be taken into account in calculations. The reason is that the mechanisms ruling the creation and reduction of vortices are not fully recognized yet. The vortex structures were mainly observed in shear zones (they appear prior to shear banding) which are fundamental phenomena observed in granular soils under drained and undrained conditions [10-14]. Since the micromechanical behaviour and fabric properties of granular materials are inherently discontinuous, heterogeneous and non-linear, the application of the discrete element method DEM, which represents the material as an assemblage of independent grains interacting with one another, has immediate physical

appeal. DEM became more and more popular nowadays for modelling granular materials due to an increasing speed of computers, a connection to the finite element method [15], its usefulness in multi-scale approaches [16] and a realistic reproduction of micro-scale phenomena such as: vortices, periodic volume changes, micro-bands, force chains. Their disadvantages are: high computational cost, inability to model grain shape accurately and difficulty to validate it experimentally.

The objective of this paper is to present the comprehensive 2D studies by DEM of vortex and anti-vortex-structures in sand behind a rigid wall during its quasi-static passive translation by taking shear localization into account. We developed 3 different methods to identify swirling patterns of particle motions in the form of vortex- and anti-vortex-structures-structures from a displacement field in two dimensions. In order to accelerate the computation time, some simplifications were assumed: large cylindrical elements with contact moments, linear sphere distribution, linear normal contact model and no particle breakage. A three-dimensional discrete model YADE developed at University of Grenoble was applied [17,18]. The discrete calculations were solely carried out with initially dense sand. The paper consists of two main parts. In the first part, discrete elements results of a passive earth pressure were summarized to show the capability of DEM to realistically simulate shear localization in sand. In the second part, the formation of vortex structures was discussed. The evolution of these structures was compared with the evolution of force chains, contact forces, sphere contacts, local void ratio, grain rotations and grain displacements.

2 DISCRETE MODEL

In order to simulate the behaviour of real sand, a three-dimensional spherical discrete model YADE was developed at University of Grenoble [17,18] by taking advantage of the so-called soft-particle approach (i.e. the model allows for particle deformation which is modelled as an overlap of particles). A linear elastic normal contact model was used only. A choice of a very simple linear elastic normal contact was intended to capture on average various contacts possible in real sands. The normal and tangential forces were linked to the displacements through the normal stiffness K_n and tangential stiffness K_s (Fig.1A). The unloading was assumed to be purely elastic (Fig.1C). The frictional sliding starts at the contact point when the contact forces $\vec{F}_s$ and $\vec{F}_n$ satisfy the limit Coulomb condition (Fig.1Aa). No forces were transmitted when grains were separated. The elastic contact constants were specified from the experimental data of a triaxial compression sand test and could be related to the modulus of elasticity of grain material E and its Poisson ratio ν [19,20].

In order to increase the rolling resistance of pure spheres to better describe the grain kinematics encountered in real irregularly shaped grains (e.g. sand), contact moments were introduced [21-23]. The normal force was assumed to contribute to the rolling resistance. The contact moment increments were calculated by means of the rolling stiffness K_r multiplied by the angular rotational increment vectors $\Delta\vec{\omega}$ (Fig.1B). To dissipate excessive kinetic energy in the discrete system, a simple local non-viscous damping scheme was adopted [24], by assuming a change of forces and moment reduced due to the damping effect specified by the parameter α. Note that the effect of damping is insignificant in quasi-static calculations [20].

Although a non-linear contact law is more realistic, a linear contact law provides similar results with the significantly reduced computation time [20] and therefore was used in the

present simulations. The five main local material parameters are necessary in our discrete simulations: E_c (modulus of elasticity of the grain contact), ν_c (Poisson's ratio of the grain contact), μ (inter-particle friction angle), β (rolling stiffness coefficient) and η (limit rolling coefficient). In addition, a particle radius R, particle mass density ρ and numerical damping parameter α are required.

The discrete material parameters of DEM ($E_c, \nu_c, \mu, \beta, \eta$ and α) were calibrated using the corresponding homogeneous axisymmetric triaxial laboratory test results on Karlsruhe sand with the different initial void ratio and lateral pressure by Wu [25]. The index properties of Karlsruhe sand are: mean grain diameter d_{50}=0.50 mm, grain size between 0.08 mm and 1.8 mm, uniformity coefficient U_c=2, maximum specific weight γ_d^{max}=17.4 kN/m^3, minimum void ratio e_{min}=0.53, minimum specific weight γ_d^{min}=14.6 kN/m^3 and maximum void ratio e_{max}=0.84. The sand grains are classified as sub-rounded/sub-angular. The procedure for determining the discrete material parameters was described by Kozicki et al. [19,20].

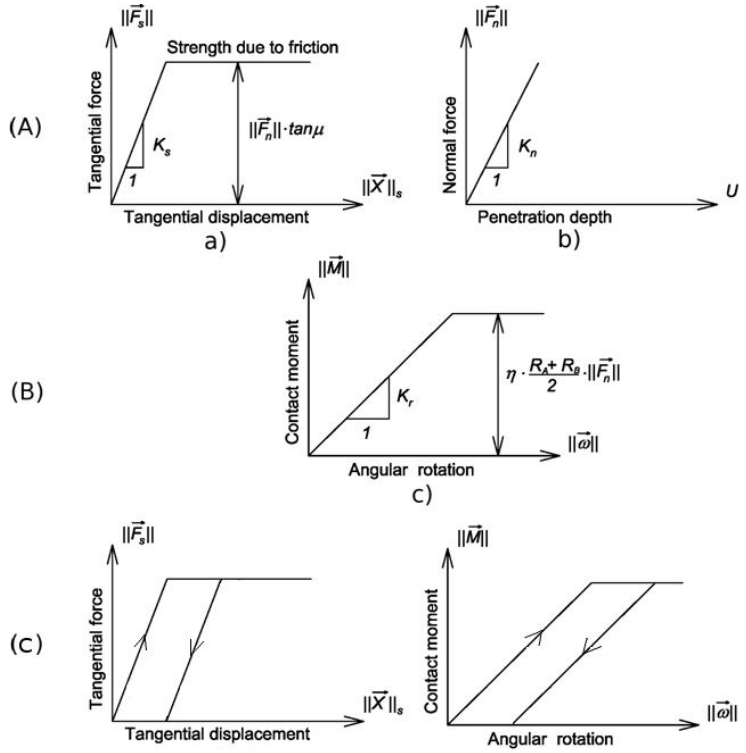

Figure 1: Mechanical response of linear contact model without (A) and with contact moments (A+B): a) tangential contact model, b) normal contact model and c) rolling contact model and C) loading and unloading path (tangential and rolling contact) wherein $\vec{F}_s$ - tangential force vector between elements, $\vec{F}_n$ - normal force vector between element, $\vec{M}$ - contact moment vector, K_s - tangential stiffness, K_n - normal stiffness, K_r - rolling stiffness, U - penetration depth, $\vec{X}_s$ - tangential displacement vector, $\vec{\omega}$- angular rotation vector, μ - inter-particle friction angle, η - limit rolling coefficient [17], [18].

3 DISCRETE MODELLING RESULTS OF PASSIVE EARTH PRESSURE MODEL TESTS

The DEM calculations were performed for a sand body of 0.40 m length and 0.20 m height in order to compare with experiments with Karlsruhe sand (d_{50}=0.5 mm) [26,27]. The vertical retaining wall and the bottom of the granular specimen were assumed to be stiff and very rough, i.e. there was no relative displacement along vertical and bottom surface [9,27]. Since the experiments were idealized as a 2D boundary value problem [26] and the effect of the specimen depth in out of plane direction turned out to be almost negligible during direct shearing in DEM calculations [28], in order to significantly accelerate simulations, the computations were performed mainly with the specimen depth equal to the grain size (i.e. one layer of spheres was simulated only).

The spheres with d_{50}=1.0 mm, characterized by a linear grain size distribution, were assumed (grain size range 0.5-1.5 mm, 62'600 spheres). The initial void ratio of sand, obtained by generating random spheres above a box and then allowing them to fall down by gravity, was e_o=0.62. The loading speed was slow enough to ensure that the tests were conducted under quasi-static conditions. The calculated inertial number (which quantifies the significance of dynamic effects) in the analyses was below 10^{-3}, what corresponds to a quasi-static regime [29]. The calculations were carried out using parameters based on triaxial compression: E_c=0.3 GPa, ν_c=0.3, μ=18°, β=0.7, η=0.4, ρ=2.55 g/cm^3 and a=0.08. The CPU computation time was about 30 days using PC 3 GHz.

Figure 2A shows the evolution of the resultant normalized horizontal earth pressure force (earth pressure coefficient) $K_p=2E_h/(\gamma h^2 d_{50})$ versus the normalized horizontal wall displacement u/h (h=0.2 m, E_h – the horizontal force acting on the wall) from plane DEM simulation. The normalized horizontal earth pressure force evolves typically for initially dense granulates in biaxial compression, triaxial compression and shearing. The specimen exhibits on average the initial strain hardening up to the peak (u/h=0.04), followed by some softening before the common asymptote is reached. The force strongly fluctuates after the peak that can be attributed to the build-up and collapse of force chains - the main carrier of stresses transferred within the granular assembly [9]. The earth pressure coefficient is K_p^{max}=3. It can be thus anticipated that for d_{50}=0.5 mm (real sand), K_p^{max} should be about 25-27. The value of K_p^{max}=30 for d_{50}=1 mm is a little bit-smaller than K_p^{max}=31 obtained by FEM (d_{50}=0.5 mm) [27] and closer to the engineering earth pressure coefficients [30].

The distribution of single sphere rotations ω during wall translation is presented in Fig.2B (red denotes the sphere rotation ω>+30° and blue ω<-30°, dark grey is related to the sphere rotation in the range 5°≤ω≤30° and light grey to the range -30°≤ω≤-5°, positive sign means clockwise rotation). All grains rotating within the range -5°≤ω≤5° are medium grey. Accepting such colour convention makes shear zones clearly observable (only particles within shear zones significantly rotate). There exists a clear grain separation regarding clockwise (red) and anti-clockwise (blue) rotation; the vast majority of 'red grains' is located within the dominant shear zone, while the vast majority of 'blue grains' is placed within the secondary radial shear zone (however there exists also a small amount of blue grains within the 'red shear zone' and *vice versa*). There is a qualitative agreement between DEM simulations and real experiments [27,31,32].

In order to determine the thickness of the shear zone, the assumption was made in this paper that the edges of a shear band are defined by an arbitrarily chosen amount of grain rotation, namely by the condition $|\omega|>5^o$. The shear zone thickness measured along the main curved shear zone at the mid-region at the residual state is: $t_s \approx 20$ mm ($20 \times d_{50}$) for d_{50}=1.0 mm. The mean inclination of the main curved shear zone to the horizontal is about 40^o in the case of DEM results, and is close to the experimental values of 35^o-40^o [27]. The maximum calculated single sphere rotation ω is about 75^o at u/h=0.15 (Fig.2B). The inclination of the radial shear zone to the vertical is 50^o. Except of the main shear zones, there exist also other faintly visible localized zones. The detailed DEM outcomes may be found in [16].

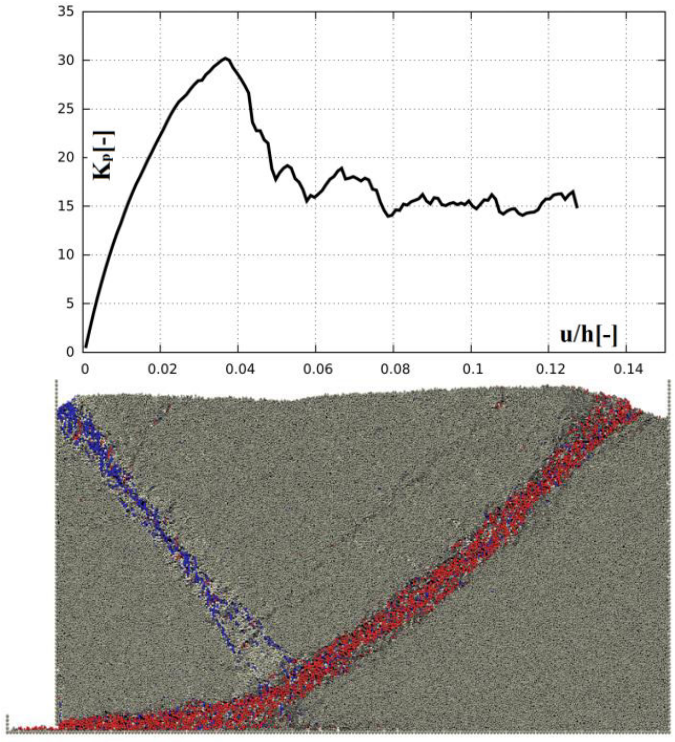

A) B)

Figure 2: DEM results (passive case, translating wall): A) evolution of resultant normalized horizontal earth pressure force $2E_h/(\gamma h^2 d_{50})$ versus normalized horizontal wall displacement u/h and B) deformed granular body 0.2×0.4 m^2 with distribution of rotation for initially medium dense sand (γ=25.5 kN/m^3, h=0.2 m, e_o=0.62, d_{50}=1.0 mm, red colour denotes clockwise rotation $\omega>+30^o$, blue colour denotes anticlockwise rotation $\omega<-30^o$)

4 DETECTION OF VORTEX STRUCTURES

The vortex structures are equivalent with the fluctuation of the grain displacements which are usually calculated from the difference $\vec{V}_i - \vec{V}_{avg}$ between the displacement vector of each sphere and the average background translation corresponding to the homogeneous (affine) strain in the specimen. The vector $\vec{V}_i$ represents the increment of sphere displacements and $\vec{V}_{avg}$ is the average sphere displacement in the granular specimen.

The difference $\vec{V}_i - \vec{V}_{avg}$ was assumed to be equal to 10'000 iteration increments (that corresponded to the normalized wall horizontal displacement increment u/h=0.002). The

structures of vortices had the tendency to occur and to disappear in the course of deformation. The vortices along the radial shear zone were not calculated because of an insufficient magnitude of displacements within this zone (Fig.3). Looking at the curved shear zone, several clockwise rotating vortices (k=13) occurred along the shear zone (in agreement with the zone shear direction) having the diameter of about the shear zone width t_s (t_s=20×d_{50}). The distance between the vortices was variable – some of them were close to each other (at the distance of t_s) or far from each other (at the distance of about 4×t_s).

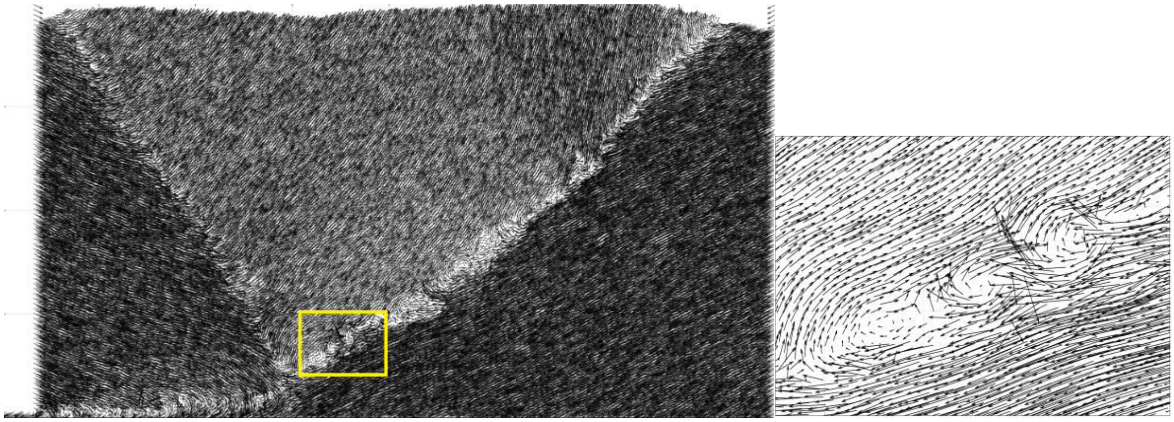

Figure 3: DEM results of displacement fluctuations of single spheres in granular specimen for u/h=0.084 (well visible vortex formation in curved shear zone in marked region) (vectors are multiplied by 50)

In order to detect vortex-structures, 3 different methods were used: 1) based on the mean pure rigid body rotation (called method '1'), 2) based on tangential displacement fluctuation vectors of spheres (called method '2'),3) based on orientation angles of displacement fluctuation vectors of spheres (called method '3').

4.1 Method "1"

It was assumed that a vortex was connected with the rigid body rotation (spin) which was calculated by the usual formula (Fig.4): $R = 0.5(\frac{\Delta u_x}{\Delta y} - \frac{\partial \Delta u_y}{\Delta x}) = 0.5(Rx,y - Ry,x)$ with $R_{x,y} = \frac{u_{x1}-u_{x0}}{a_c} + \frac{u_{x3}-u_{x0}}{-a_c}$ and $R_{y,x} = \frac{u_{y2}-u_{y0}}{a_c} + \frac{u_{y4}-u_{y0}}{-a_c}$. The component Δu_x denotes the mean displacement increment in the direction *'X'* (parallel to the shear zone), Δu_y denotes the mean displacement increment in the direction *'Y'* (perpendicular to the shear zone) between two neighbouring square cells and u_{xi} and u_{yi}, the displacements in these cells and a_c - the square cell side size. The average background translation vanishe in this method. The field of the rigid body rotation (equivalent to the vortex-structures) was solely calculated for the curved shear zone inclined under the angle α to the horizontal (Fig.4). In general it may be calculated for each shear zone on condition that the inclination angle of the shear zone α is known in advance. The calculation algorithm was the following:

1. The displacement field of all single spheres was changed into a regular orthogonal lattice to calculate the mean displacement of spheres in the square cells A_c=a_c×a_c at the distance of d_{50}. The cell dimension was assumed to be smaller than the shear zone thickness t_s in order to capture the entire vortex whose diameter usually was ≤t_s).

2. In order to eliminate the rigid body rotation due to pure shear (e.g. $R_{x,y}\neq 0$ and $R_{y,x}=0$ or $R_{x,y}=0$ and $R_{y,x}\neq 0$ in Eq.10), the limitation was imposed on the shear components $R_{x,y}$ and $R_{y,x}$ in the following form: $R_{x,y}/R_{y,x}\leq m$.

The field of the rigid body motion limited to the curved shear zone is shown in Fig.5 with the cell area of $A_c=0.33t_s\times 0.33t_s$ and $m=3$. There were detected 7 vortices whose location was similar as in Fig.3. However their number was smaller than in Fig.3. The small vortices were not detected or they were connected to each other.

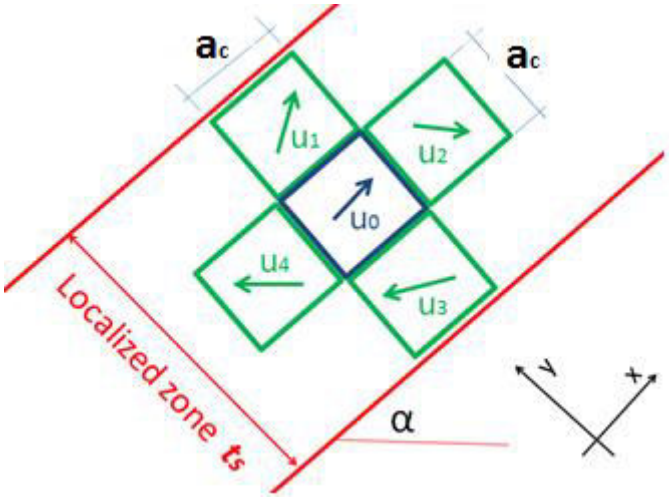

Figure 4: Schema for calculations of rigid body rotation in localized shear zone (u_i – mean displacement vector in cell area $a_c\times a_c$ (α – inclination angle of shear zone to horizontal, t_s - width of shear zone)

4.2 Method "2"

The vortices were calculated based directly on the displacement fluctuations of single spheres. The mean displacement fluctuation vector of sphere displacements in the square cell $A_c=a_c\times a_c$ (green spheres in Fig.6) in the neighbourhood of each central sphere (blue sphere in Fig.6) was decomposed into 2 vectors: the normal $\boldsymbol{n}$ and tangential $\boldsymbol{t}$ with respect to its movement direction. If the neighbouring spheres had a tangential displacement fluctuation component only, the blue sphere was assumed to be the vortex mid-point. The movement normal component moved solely the spheres closer or further from each other.

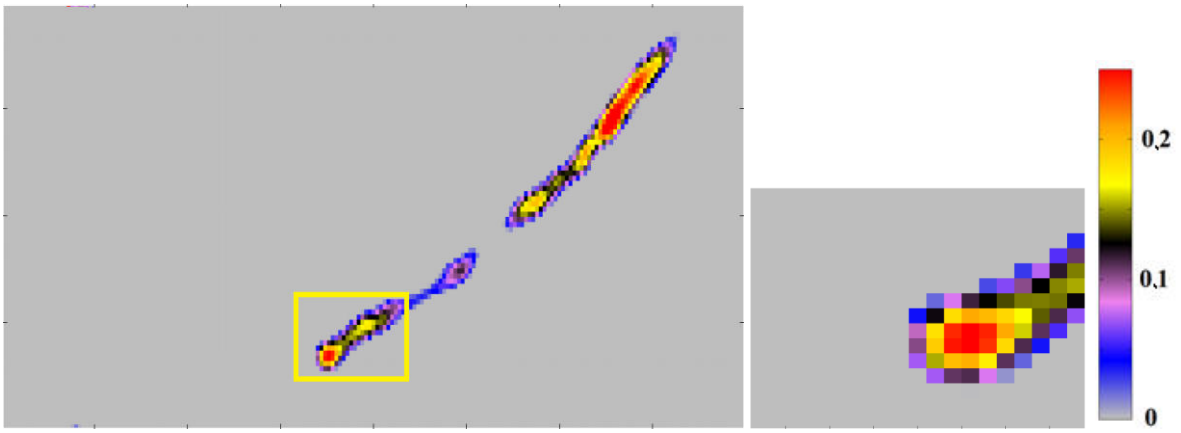

Figure 5: Map of spin *A* (Eqs.10-11) in curved shear zone using method '1' (u/h=0.084): a) entire specimen and b) zoom on marked region (red colour correspond to high rigid body rotation)

The vortex strength was determined as the sum of the tangential displacement fluctuation vectors of surrounding spheres for each single sphere. The anti-vortex strength was described as the sum of the absolute value of the tangential vectors of surrounding spheres. In order to avoid pure shear, the sum of the tangential displacement vectors was assumed to be higher than the sum of the normal displacement vectors: $\Sigma u_t/\Sigma u_n>m$. The average background translation was calculated for the entire granular specimen ($a_c=t_s$, m=2). There were 13 clock-wise vortices (as in Fig.3) and 2 anti-clock-wise vortices in the curved shear zone (Fig.7). The vortex size varied between 10-26 mm (the mean value was 18 mm$\approx t_s$).

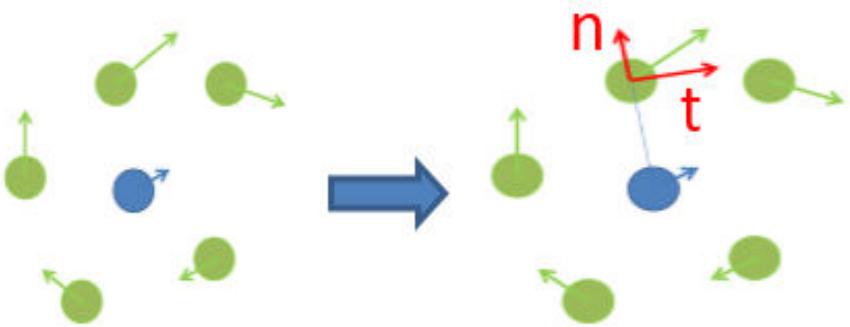

Figure 6: Decomposition of displacement vector ***v*** of green spheres surrounding main blue sphere into normal ***n*** and tangential ***t*** vector to its movement

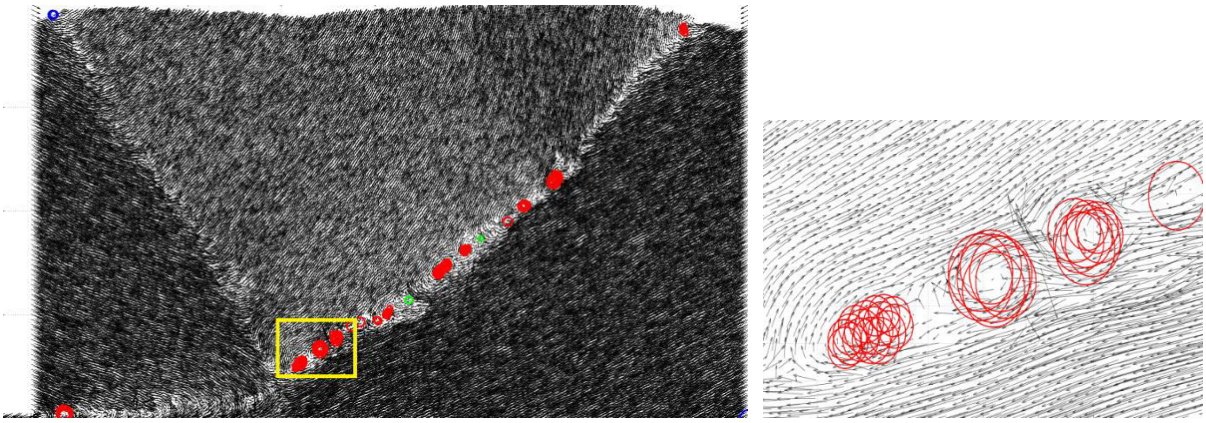

a) b)

Figure 7: Displacement fluctuation vector field with marked vortices from DEM using method '2' (u/h=0.084): a) entire specimen and b) zoom on marked region (red circles correspond to clock-wise vortices, blue circles to anti-clock-wise and green circle to anti-vortices)(vectors are multiplied by 50)

4.3 Method "3"

A special method used in the physics was applied, based on the orientation angles of the displacement fluctuation vectors of neighbouring single spheres was used [33]. Initially the displacement fluctuation field of irregularly distributed spheres was changed into a regular orthogonal lattice by calculating the mean displacement fluctuations of spheres inside the square cell $5d_{50}\times5d_{50}$ at the points spaced by the d_{50}-distance in the both directions on the 2D grid. In order to find the centre of a vortex, a group of 4 angles (spins) was chosen which were the corners of the square $d_{50}\times d_{50}$ on the 2D grid. Each corner was the result of the average displacement fluctuation from the square $A_c=5d_{50}\times5d_{50}$**.** The set of 4 spins was chosen to determine whether they rotated by $\pm2\pi$ as the eye went from one spin to the next in a clockwise or an anti-clockwise direction around the square (Fig.8). The vortex was detected in the lattice when the spins of the normalized displacement fluctuation vectors rotated by at least 2π, i.e.

$$-2.01\pi < \Sigma\alpha_i=\alpha1+\alpha2+\alpha3+\alpha4 < -1.99\pi \quad (1)$$

as the eye moved clockwise around the closed path (Fig8a) or 2π, i.e.

$$1.99\pi < \Sigma\alpha_i=\alpha1+\alpha2+\alpha3+\alpha4 < 2.01\pi \quad (2)$$

in the anti-clockwise direction (Fig.8n). Note that the vector length was ignored. In turn, the anti-vortex (equivalent with shear, Fig.8d) might occur if $\Sigma\alpha_i=-2\pi$ as the eye moved in an anti-clockwise direction or $\Sigma\alpha_i=2\pi$ as the eye moved in a clockwise direction (it could also be left- and right-handed). In order to describe the vortex type, two checks were always carried out; one in the clockwise and one in the anti-clockwise direction. Usually, only one check satisfied the conditions in Eqs.1 and 2. However, very rarely this condition was twice satisfied due to the assumed range equal to 0.02π. In order to eliminate the frequency noise (caused by the fact that spins rapidly and chaotically changed their directions as the eye moved to the next one), the maximum allowed angle which varied between the neighbouring corners was taken as $\leq160^o$ (Fig8a), If any angle between two neighbours was larger than 160^o , the check in the cell was aborted. One may also use the approach with a higher number of vectors around the selected point 'p' - e.g. with 8 vectors (Figs.8c and 8d) that allows for determining more vortices.

The results are shown in Fig.9 (for 4-vector approach). This method allows for capturing for very small vortices. In the curved shear zone 22 vortex-structures were found for the average background translation calculated for entire granular specimen (Fig.9) against 13 in Fig.3. Some vortices were close to each other and create a large structure composed of 2-4 vortices.

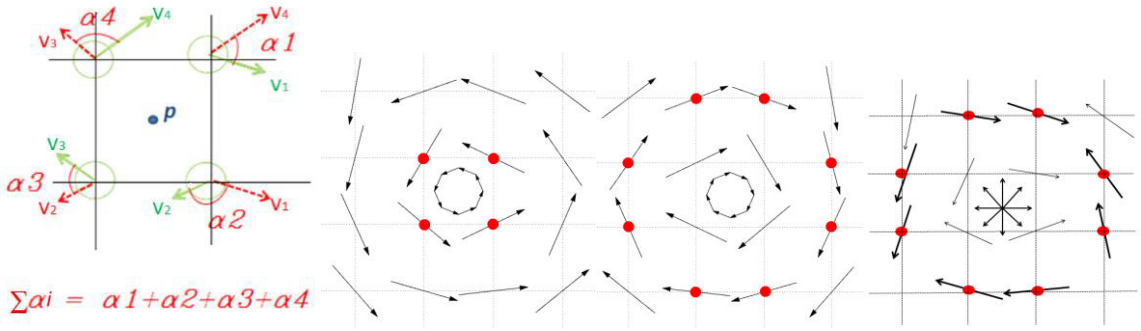

a) b) c) d)

Figure 8: The displacement fluctuation vectors of single spheres using method '3' (p - sphere in mid-point): a) orientation angles α_i, b) 4-vector approach to determine left-handed vortex, c) 8-vector approach to determine right-handed vortex and d) 8-vector approach to determine right-handed anti-vortex (distance between spins is d_{50})

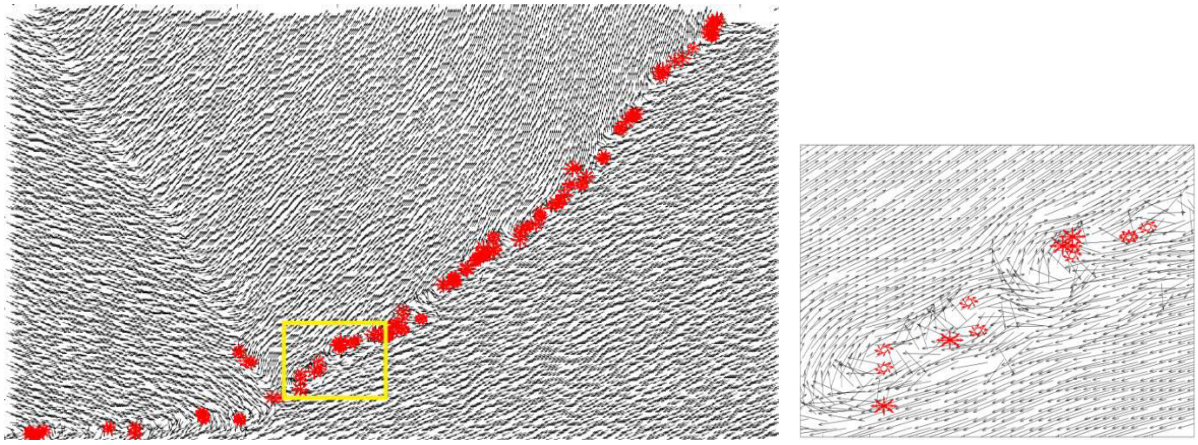

a) b)

Figure 9: Displacement fluctuation vector field with marked vortices from DEM using method '3' (u/h=0.084): a) entire specimen and b) zoom on marked region (circles correspond to vortices and stars correspond to anti-vortices, black arrows correspond to mean displacement fluctuation field)

5 CONCLUSIONS

The following conclusions can be drawn from our DEM analyses of a pattern of shear zones during a passive earth pressure problem:

- DEM, which directly takes micro-structures of granular bodies into account, realistically predicts the experimental results of a pattern of shear zones in the interior of initially medium dense sand behind a retaining wall. Grain rotations are noticeable only in shear zones.

- In shear zones, vortex structures systematically occur which are a direct manifestation of grain rearrangement. The number of the detected vortices was the highest in the method "3" which did not take into account the length of the displacement vector.

Acknowledgment

The authors would like to acknowledge the support by the grant 2011/03/B/ST8/05865 "*Experimental and theoretical investigations of micro-structural phenomena inside of shear localization in granular materials*" financed by Polish National Research Centre.

REFERENCES

[1] Utter B, Behringer RP. Self-diffusion in dense granular shear flows. *Phys. Rev. E*. (2004); 69(3), 031308-1–031308-12.

[2] Abedi S, Rechenmacher AL, Orlando AD. Vortex formation and dissolution in sheared sands. *Granular Matter* (2012); 14: 695-705.

[3] Richefeu V, Combe G, Viggiani G. An experimental assessment of displacement fluctuations in a 2D granular material subjected to shear. *Geotechnique Letters* (2012); 2: 113–118.

[4] Radjai F, Roux S. Turbulent-like fluctuation in quasi-static flow of granular media. *Phys. Rev. Lett.* (2002); 89, 064302.

[5] Rognon P, Einav I. Thermal transients and convective particle motion in dense granular materials. *Phys. Rev. Lett.* (2010), 105(21), 218301.

[6] Williams JR, Rege N. Coherent vortex structures in deforming granular materials. *Mechanics of Cohesive-frictional Materials* (1997); 2: 223-236.

[7] Peters JF, Walizer LE. Patterned nonaffine motion in granular media. *Journal of Engineering Mechanics* (2013); 139, 10: 1479-1490.

[8] Tordesillas, A., Pucilowski, S., Lin, Q, Peters, J.F., Behringer, R. P. Granular vortices: identifuication, characterization and conditions for the localization of deformation. *Journal of Mechanics and Physics of Solids,* (2015).

[9] Nitka, M., J. Tejchman, J., Kozicki, J. and Leśniewska,' D. DEM analysis of micro-structural events within granular shear zones under passive earth pressure conditions. *Granular Matter*, (2015), doi: 10.1007/s10035-015-0558-0.

[10] Desrues J, Viggiani C. Strain localization in sand: over- view of the experiments in Grenoble using stereophotogrammetry. *J. Numer. Anal. Methods Geomech.* (2004); 28(4):279–321.

[11] Gudehus G., Nűbel K. Evolution of shear bands in sand. *Geotechnique* (2004); 113 54(3):187–201.

[12] Tejchman J. *FE modeling of shear localization in granular bodies with micro-polar hypoplasticity*. Springer Series in Geomechanics and Geoengineering (eds. Wu and Borja), Springer Verlag, Berlin-Heidelberg, (2008).

[13] Tejchman, J., Gorski J. Computations of size effects in granular bodies within micro-polar hypoplasticity during plane strain compression. *Int. J. Solids Struct*. (2008); 45(6):1546–1569.

[14] Gudehus G. *Physical Soil Mechanics,* Springer, (2011).

[15] Rojek J. Discrete element modelling of rock cutting. *Computer Methods in Materials Science* (2007); 7, 2**:** 224–230.
[16] Nitka M, Combe G, Dascalu C, Desrues J. Two-scale modeling of granular materials: a DEM-FEM approach. *Granular Matter* (2011), 13, 277-281.
[17] Kozicki J, Donze FV. A new open-source software developed for numerical simulations using discrete modelling methods. *Computer Methods in Applied Mechanics and Engineering* (2008); 197, 4429-4443.
[18] Šmilauer V, Chareyre B. *Yade DEM Formulation*. Manual, (2011).
[19] Kozicki J, Tejchman J, Mróz Z. Effect of grain roughness on strength, volume changes, elastic and dissipated energies during quasi-static homogeneous triaxial compression using DEM. *Granular Matter* (2012), 14(4):457-468.
[20] Kozicki J, Tejchman J., Műhlhaus HB. Discrete simulations of a triaxial compression test for sand by DEM. *Int. J. Num. Anal. Methods in Geomech.* (2014); 38, 1923-1952.
[21] Iwashita K, Oda M. 1998. Rolling resistance at contacts in simulation of shear band development by DEM. *ASCE J Eng Mech*, 124(3), 285–92.
[22] Jiang MJ, Yu H-S, Harris D. 2005. A novel discrete model for granular material incorporating rolling resistance. *Computers and Geotechnics* 32, 340-357.
[23] Mohamed A, Gutierrez M. Comprehensive study of the effects of rolling resistance on the stress-strain and strain localization behaviour of granular materials. *Granular Matter* 12 (2010) 5, 527-541.
[24] Cundall PA, Hart R. Numerical modeling of discontinua. *J. Eng. Comp*. (1992); 9: 101–113.
[25] Wu W. Hypoplastizität als mathematisches Modell zum mechanischen Verhalten granularer Stoffe. *Heft 129, Institute for Soil- and Rock-Mechanics, University of Karlsruhe*, (1992).
[26] Gudehus G and Schwing E. Standsicherheit historischer Stützwände. *Internal Report of the Institute of Soil and Rock Mechanics*, (1986), University Karlsruhe.
[27] Tejchman J. FE modeling of shear localization in granular bodies with micro-polar hypoplasticity. *Springer Series in Geomechanics and Geoengineering (eds. Wu and Borja), Springer Verlag*, Berlin-Heidelberg (2008).
[28] Kozicki J, Niedostatkiewicz M, Tejchman J, Mühlhaus H.-B. Discrete modelling results of a direct shear test for granular materials versus FE results. *Granular Matter* (2013), 15, 5: 607-627.
[29] Roux, J.N., Chevoir, F. Discrete numerical simulation and the mechanical behaviour of granular materials. *Bulletin des Laboratoires des Ponts et Chaussees* 254 (2005), 109-138.
[30] Gudehus, G. *Erddruckermittlung. Grundbautaschenbuch*, Teil 1, Ernst und Sohn. 1996.
[31] Lucia J.B.A.Passive earth pressure and failure in sand. *Research Report,* University of Cambridge (1966).
[32] Niedostatkiewicz M, Leśniewska D, Tejchman J. Experimental analysis of shear zone patterns in sand for earth pressure problems using Particle Image Velocimetry. *Strain*, 47, (2011) ,s2, 218-231.
[33] Gould H, Tobochnik J, Christian W. Introduction to Computer Simulation Methods: Application to Physical Systems (3rd edition), chapter 15, page 655.